The monoenergetic unimolecular reaction of expansion-cooled NO_2: NO product state distributions at excess energies 0–3000 cm^{-1}

M. Hunter, S. A. Reid, D. C. Robie,[a] and H. Reisler
Department of Chemistry, University of Southern California, Los Angeles, California 90089-0482

(Received 4 March 1993; accepted 9 April 1993)

We report detailed vibrational, rotational, and electronic (V,R,E) distributions of nascent $NO(X\,^2\Pi_{1/2,3/2})$ deriving from monoenergetic unimolecular reactions of expansion-cooled NO_2. Near UV excitation above dissociation threshold (25 130.6 cm^{-1}) prepares molecular eigenstates which are admixtures of the optically active $1\,^2B_2$ state and the ground $\tilde{X}\,^2A_1$ electronic state. The strong mixings among the vibronic states result in vibrational predissociation from states of predominantly ground state character, and the NO product state distributions (PSDs) are compared with the predictions of several statistical theories. The PSDs are combined with previously measured $O(^3P_J)$ distributions and unimolecular reaction rates, thereby providing a complete description of the decomposition of NO_2 at these excess energies. All the rotational distributions show prominent fluctuations and structures, but tend on average to follow the statistical distributions predicted by phase space theory (PST). This behavior is observed in both $NO(v=0)$ and $NO(v=1)$ channels, although the relative population in $NO(v=1)$ was always greater than expected by PST. The $NO(v=1)$ fractional population is bounded by the predictions of the separate statistical ensembes (SSE) method, and recent variational Rice–Ramsperger–Kassel–Marcus (RRKM) calculations are in agreement with the experimental results. Prior distributions underestimate the degree of vibrational excitation even more than PST does, and also the relative populations of the lower NO rotational levels. The observed NO spin–orbit states are always colder than statistical. We conclude that a significant interplay between dynamical biases and statistical expectations is manifest from the onset of dissociation, and is particularly evident when the initial parent rotational state is well defined.

I. INTRODUCTION

NO_2 is one of the smallest molecules whose unimolecular reaction can be studied continuously as a function of excess energy $E^\dagger$ above its ground state dissociation threshold D_0. With its small density of states and relatively small number of product channels, it can provide a stringent test for the limits of applicability of statistical theories, the basic tenets of each theory and the interplay between statistics and dynamics in unimolecular decay.

Extensive data are available for the monoenergetic simple-bond-fission unimolecular reactions of three other small molecules NCNO,[1–4] CH_2CO,[5–9] and H_2O_2.[10–15] In the latter case, there are still questions regarding complete intramolecular vibrational redistribution (IVR) prior to dissociation, and comparisons with statistical theories are not straightforward. However, both NCNO and CH_2CO decay have been well described within the framework of statistical theories, such as phase space theory (PST),[16–18] the separate statistical ensembles (SSE) method,[2] and the variational Rice–Ramsperger–Kassel–Marcus (RRKM) theory.[19] In the case of NCNO, e.g., no deviations from statistical behavior have been observed even for correlated product state distributions (PSDs), i.e., for internal energy distributions of NO which correlate with specific rovibrational states of CN.[3] Variational RRKM theory, which requires knowledge of the potential energy surface (PES), is the most difficult computationally, but so far is the only theory that describes successfully the rates *and* the PSDs for both NCNO and CH_2CO decay—an important accomplishment.[19] The success of statistical theories in modeling these decay processes is remarkable, suggesting a high degree of vibrational energy randomization prior to dissociation even in such fast dissociating small molecules.

NO_2 provides a unique case for further testing statistical theories. Its vibronic density of states around $D_0(\rho < 2/cm^{-1})$[20–23] is over two orders of magnitude smaller than for NCNO, and its dissociation lifetime is very short, ranging from a few picoseconds near threshold to less than a vibrational period at photolysis wavelengths < 330 nm ($E^\dagger > 5000\ cm^{-1}$).[23–25] However, there are strong vibronic couplings between the optically accessible $1\,^2B_2$ state and high vibrational levels of the $\tilde{X}\,^2A_1$ ground state,[22,26–34] facilitated by a conical intersection near the $1\,^2B_2$ minimum,[32] and there is evidence for the onset of vibronic and even rovibronic chaos below D_0.[22,35] Hence, it is reasonable to expect vibrational predissociation from states with highly mixed rovibrational character, justifying the use of statistical theories.

Several workers have investigated the photodissociation of NO_2 at low $E^\dagger$, but there is still no consensus regarding the statistical nature of the decay. Busch and Wilson, in pioneering studies of photofragment translational energy distributions from NO_2 photolysis, proposed a nonstatistical decay mechanism.[36] Their time-of-flight analysis of the NO and O products from $\lambda = 347.1$ nm photolysis ($E^\dagger = 3679\ cm^{-1}$) indicated that the $NO(v=0)$ and

[a]Present address: Department of Chemistry, Barnard College, New York, NY.

$NO(v=1)$ channels are approximately equally populated, thus deviating from the predictions of simple statistical theories such as PST. A similar conclusion was reached by Welge and co-workers, based on NO R, V, and E distributions following photolysis of 300 K NO_2 samples at $\lambda=351$, 337, and 308 nm ($E^\dagger=3359$, 4534, and 7337 cm^{-1}, respectively).[37] The NO vibrational populations were found to be inverted at $\lambda=351$ and 337 nm, and the rotational distributions were consistently bimodal, showing a "cold" component at low J_{NO} (<120 K), and a "hot" distribution for the higher J_{NO} rotational levels (>1000 K). In addition, the $NO(^2\Pi_\Omega;\Omega=1/2,3/2)$ spin–orbit distributions were found to be "colder" than statistical at all photolysis wavelengths and to vary for each NO product vibrational channel. Bimodal rotational distributions were also observed at very low excess energies in experiments performed by Robra *et al.* in a supersonic molecular beam ($E^\dagger<130$ cm^{-1}; $T_{rot}(NO_2)<10$ K).[21,38] Attempts to model their rotational distributions with microcanonical prior calculations were unsuccessful, except at a single photolysis energy ($E^\dagger=126$ cm^{-1}). Similarly, in NO_2 photolysis studies in an effusive beam at $\lambda=376.3$ nm ($E^\dagger=1444$ cm^{-1}), Kawasaki *et al.* found the NO rotational distributions to be well fit by two separate Boltzmann temperatures (280 K for the lower J_{NO} levels and 1300 K for high J_{NO}). These results suggested that at least two different decay channels are available for NO_2 photofragmentation at low $E^\dagger$.[39] A kinematic model, e.g., has been proposed by Chen and Pei to account for the bimodal NO rotational distributions observed by Welge *et al.* at 337 nm.[40]

Evidence for dynamical effects in NO_2 photodissociation has also been found in the relative yields of the $O(^3P_J)$; $J=2,1,0$) spin–orbit levels as a function of photolysis energy. Miyawaki *et al.*, in experiments using jet-cooled NO_2 ($T_{rot}<1$ K), measured these branching ratios continuously in the range $E^\dagger=0$–2200 cm^{-1} and found them to fluctuate strongly around an average ratio much colder than statistical.[20] Furthermore, in a similar study at $\lambda=355$ nm ($E^\dagger=3038$ cm^{-1}), Rubahn *et al.* found the $O(^3P_J)$ spin–orbit ratios to be directly influenced by the NO_2 parent rotational state; they observed that reducing the NO_2 temperature in the molecular beam resulted in colder $O(^3P_J)$ spin–orbit distributions.[41] These "anomalous" $O(^3P_J)$ ratios cannot be reconciled with statistical theories—including PST, which explicitly incorporates total angular momentum constraints.

In contrast to these studies, other experiments performed at similar excess energies are in good agreement with statistical expectations. Troe and co-workers first proposed that a statistical theory, the statistical adiabatic channel model (SACM), can account for the variation of the decomposition rates of 300 K NO_2 samples as a function of photolysis energy at $E^\dagger=0$–2500 cm^{-1}.[24] The decay rates in their experiment $k(E)$ were extracted only indirectly from collisional quenching rates at high pressures. However, these decay rates have recently been measured directly with subpicosecond resolution by Ionov *et al.*, and found to be in accord with Troe's results and with the expectations of RRKM theory.[23] A step-like structure in the dependence of $k(E)$ on $E^\dagger$ was observed when the experiment was performed with jet-cooled samples, and this was interpreted in terms of the vibrational structure of the transition state (TS), and falls within the framework of statistical theories.[23] A statistical outcome was also found by Mons and Dimicoli in the $NO(v=1)$ rotational distributions obtained with 300 K samples, at $E^\dagger<3600$ cm^{-1}, which could be well fit by microcanonical prior distributions.[42] Their results also agree with a more refined, RRKM-type statistical model implemented by Elofson *et al.*, in which angular momentum constraints—which are not included in prior calculations—are explicitly taken into account.[43]

In light of these conflicting interpretations, it is clear that many questions regarding the decomposition of NO_2 still remain. Can the photodissociation be described as a statistical process? Would dynamical effects become increasingly evident at short dissociation times and higher excess energies? What is the influence of the initial parent rotational state, or of the $1\,^2B_2/\tilde{X}\,^2A_1$ conical intersection, on the dissociation dynamics? Would the small number of final product states help reveal underlying dynamical biases?

In this paper, we address some of these issues by examining the applicability of statistical theories to model the $NO(v=0,1)$ R, V, and E distributions from photolysis of expansion-cooled NO_2 ($T_{rot}<10$ K) at $E^\dagger=0$–3100 cm^{-1} above $D_0=25\,130.6$ cm^{-1}.[21,44] The dependence of the NO vibrational distributions on $E^\dagger$ near the $NO(v=1)$ threshold, and its comparison with statistical expectations, is of particular significance since it has not been previously reported. Mons and Dimicoli were unable to extract NO vibrational distributions due to the large presence of background $NO(v=0)$ in their 300 K NO_2 samples[42]; thus, the lowest excess energy at which a vibrational distribution had been previously measured with 300 K samples was ~1500 cm^{-1} above the $NO(v=1)$ threshold (at $\lambda=351$ nm), where it was found to be inverted.[37] In addition, our experiments were performed under expansion-cooled conditions, which removed the extensive thermal averaging over NO_2 initial states inherent in 300 K samples and thus provided a more stringent test of the statistical theories. In particular, the selectivity obtained in initial NO_2 angular momentum states allowed us to demonstrate the importance of total angular momentum conservation constraints in the statistical models of unimolecular decay, especially for triatomic molecules (see below).

We have recently reported, in a preliminary communication, $NO(v=0,1)$ R and V distributions from photodissociation of jet-cooled NO_2 at two excess energies ($E^\dagger=1949$ and 1998 cm^{-1}) in the vicinity of the $NO(X\,^2\Pi_{1/2};\ v=1)+O(^3P_2)$ threshold, using resonance-enhanced multiphoton ionization (REMPI) for NO detection.[45] In the present paper, those studies are extended to $E^\dagger=0$–3000 cm^{-1}, and we use laser-induced fluorescence (LIF) detection in order to avoid saturation. Our results are compared with microcanonical prior distributions, in which total energy conservation is the only constraint;[46–48]

PST calculations, where both energy *and* total angular momentum constraints are applied,[16–18] and to the SSE/PST method and the variational RRKM theory for the determination of vibrational populations.[2,19,49] As in our previous work,[45] we find that the NO(v=0,1) rotational distributions show significant fluctuations and structures, but are well fit on average by PST. Prior distributions, on the other hand, consistently underestimate the relative populations of the lower NO rotational levels, primarily as a result of neglecting angular momentum constraints. The NO(v=0,1) vibrational distributions are always "hotter" than expected by either prior or PST, but they can still be accounted for by restricted statistical theories such as the SSE method and the variational RRKM theory.[2,19,49] In addition, there is a marked propensity for producing cold NO($^2\Pi_\Omega$; Ω=1/2,3/2) spin–orbit distributions at all excess energies.

The paper is organized as follows: Secs. II and III describe the experimental methods and results. Section IV is devoted to comparisons between the predictions of the different statistical models as they apply to NO_2 and includes examples which highlight the differences between the theories. In Sec. V, we discuss the implications of our findings to the NO_2 decomposition mechanism. Section VI provides a brief summary and concludes with the suggestion that the interplay between dynamics and statistics in NO_2 decomposition is important from its onset.

II. EXPERIMENT

Expansion-cooled NO_2 was dissociated by one-photon laser photolysis at wavelengths λ=398–355 nm, and nascent NO(v,J) distributions were monitored by LIF using the γ-band system. The experimental arrangement has been described previously in detail.[50]

A 1%–5% NO_2/He mixture, kept at a backing pressure of 700 Torr, was expanded into a vacuum chamber maintained at $<2\times10^{-5}$ Torr through a solid-nickel nozzle (0.5 mm diameter, 180 μs pulse width) which was piezoelectrically actuated. The free jet was intersected at right angles by collinear and counterpropagating photolysis and probe laser beams, approximately 15 mm downstream from the nozzle orifice. A Hamamatsu RU166H photomultiplier tube (PMT), mounted perpendicularly to both the free jet and the laser beams, collected NO fluorescence through a "solar blind" filter (Corion, 300 nm, 85 nm bandwidth). The gas mixture contained O_2, seeded in a 1:1 ratio with NO_2, to reduce the amount of background NO.[51]

Excimer laser-pumped dye laser systems were used for photolysis and detection. The tunable photolysis laser (Lambda Physik, EMG-101 MSC/LPD-3000) was operated with QUI/dioxane and butyl-PBD/dioxane dye solutions to cover the ranges 370–400 and 358–370 nm, respectively. Typical pulse energies were 3–9 mJ and the beam was loosely focused with a 1 m focal length lens to 2 mm diameter at the interaction region. For photolysis at 355 nm, the third harmonic of a Quanta Ray DCR-1A Nd:YAG laser was used. Although the pulse energies and focusing conditions were similar, the bandwidth of the tripled Nd:YAG beam ($\sim$2 cm^{-1}) was larger than that of the dye laser system (0.3–0.5 cm^{-1}).

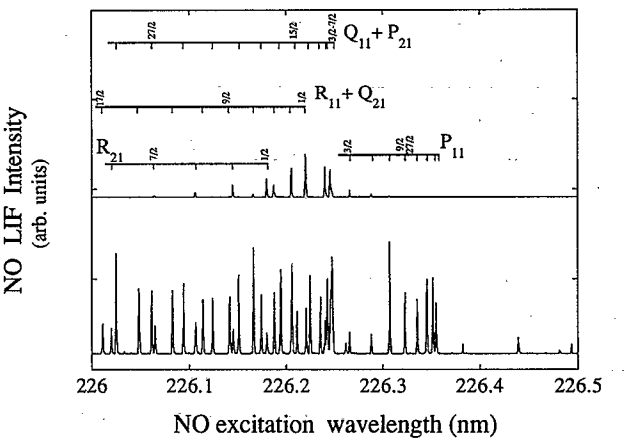

FIG. 1. A portion of the NO γ(0,0)-band LIF spectrum from NO_2 photodissociation at λ=391.8 nm ($E^\dagger$=392 cm^{-1}) showing the relative contributions to the NO LIF signal from background NO (upper panel) and from photodissociation products with the photolysis laser turned on (lower panel).

The probe beam was obtained by frequency doubling the output of a dye laser (Lambda Physik MSC 201/FL 3002) with a BBO crystal using a Coumarin-450 dye to cover the range of the NO γ(0,0) and γ(1,1) bands. The probe pulse energy was maintained at <3 μJ to avoid saturation. The probe beam was unfocused, apertured to a 5 mm diameter, and delayed 200 ns with respect to the photolysis beam. Both beams were linearly polarized with their electric field vectors perpendicular to the PMT axis.

NO (v=0,1) R,V distributions were obtained at several photolysis energies above D_0 by monitoring the LIF signal from the NO γ(0,0) and γ(1,1) bands at probe wavelengths λ_{pr}=222–227 nm. The LIF signal was normalized to both laser intensities and also corrected for the different Franck–Condon factors of the γ bands,[52] and for the wavelength dependencies of the PMT response and the filter transmission. Alignment effects were not included in the data analysis.

Figure 1 shows a portion of a typical LIF spectrum obtained at excess energy $E^\dagger$=392 cm^{-1}. Note the good signal to noise ($\sim$100:1), despite the low intensity of the probe laser beam. We emphasize that already at probe pulse energies in the range 3–10 μJ partial saturation of strong branches (e.g., $Q_{11}+P_{21}$) was observed, while the weak branches (e.g., R_{21} satellite branch) were still unsaturated. The NO product state distributions presented below were all obtained under unsaturated conditions, verified by comparing populations obtained from main vs satellite branches.

NO_2 was purified by repeated freeze–pump–thaw cycles in a dry ice/acetone slush (−76 °C) until the solid became white (typically after three cycles). Despite purification, some NO impurities were always present as thermal decomposition products in our NO_2 samples. However, by performing the experiments under expansion-

cooled conditions, the NO background was cooled to T_{rot} <10 K, and only NO molecules in the $^2\Pi_{1/2}$ state with $J\leqslant 3.5$ had significant population. This is shown in the top panel of Fig. 1, which compares the LIF signal from background NO to LIF signal when the photolysis beam was turned on. In all the NO($^2\Pi_{1/2}$, $v=0$) rotational distributions presented below, we exclude the affected NO rotational levels. The gases used were NO_2 (Matheson; >99.5% purity) (purified as described above) He (MG Industries; 99.9995%), and O_2 (Spectra Gases; 99.99%). The latter two were used without further purification.

Reducing the contribution of background NO enabled us to measure NO($v=0,1$) vibrational distributions with considerable precision. These were extracted from LIF spectra by two different methods. In one, we simply integrated over the entire $\gamma(0,0)$ and $\gamma(1,1)$ bands separately, normalizing the LIF signals to the photolysis and probe laser intensities, and correcting for the Franck–Condon and instrumental response factors. This procedure, which included direct subtraction of background NO signals, included contributions from bandheads and from unresolved, overlapped transitions. Furthermore, it took no account of the individual Hönl–London rotational line strengths, which vary dramatically among the different rotational branches and as a function of J_{NO}; hence, this approach is only valid if *all* the observed transitions are unsaturated.

The second method consisted in first extracting rotational level populations from well-resolved peaks (<10% overlap with adjacent peaks) in the LIF spectra. In this case, individual LIF peaks were integrated and normalized to their corresponding line strengths, as well as laser powers, Franck–Condon factors, and instrument response functions. Vibrational populations were then obtained by summing over these rotational level distributions for each vibrational channel. The contribution from levels missing due to overlap was estimated by extrapolation from adjacent, well-resolved levels; typically, the missing levels accounted for <5% of the total rotational population. Vibrational distributions derived by both methods agreed within our experimental uncertainty (±15%), providing further confirmation that unsaturated conditions were achieved. The experimental uncertainty reflects a 10% standard deviation in the reproducibility of the peak heights in our LIF spectra.

Under our expansion conditions, NO_2 in the free jet had a rotational temperature of 6±1.5 K at the interaction region. This was measured in a separate experiment, in which a LIF spectrum of a NO_2 vibronic band near 16 850 cm^{-1} was obtained with rotational resolution. This band has been observed by Smalley *et al.* at 16 851.2 cm^{-1} and rotationally analyzed.[53] Fluorescence was detected with a GaAs PMT through a Corning 2-64 filter. The NO_2 rotational temperature thus measured is consistent with the structure observed in the NO photofragment yield spectra at energies below D_0 (Figs. 2 and 3).[21] The rotational temperature of the background NO in the molecular beam was always measured to be slightly warmer than that of NO_2 (typically 6–8 K).

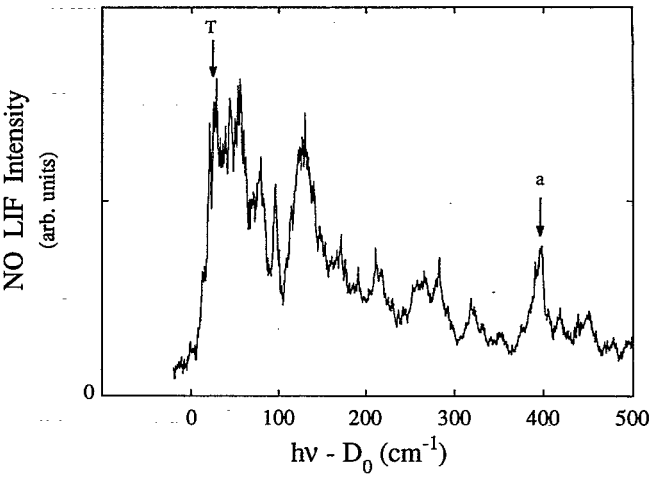

FIG. 2. Photofragment yield spectrum of NO_2 obtained by monitoring NO($X\,^2\Pi_{1/2}$, $v=0$, $J=3.5$). The $R_{11}+Q_{21}(3.5)$ line was monitored as a function of photolysis laser frequency ν. T=thermodynamic threshold for the appearance of NO($v=0$, $J=3.5$); a=excess energy where NO product state distribution was measured. $D_0=25\,130.6$ cm^{-1} is the dissociation threshold.

III. RESULTS

NO($v=0,1$) R, V, and E distributions from NO_2 photodissociation were obtained at several excess energies in the range $E^{\dagger}=0$–3000 cm^{-1} above the $O(^3P_2)+NO(^2\Pi_{1/2})$ threshold. As observed in our preliminary study,[45] *all* rotational level distributions showed prominent fluctuations to varying degrees, but tended on average to follow a statistical distribution predicted by PST. This behavior was observed in both NO($v=0$) and NO($v=1$) channels, although the relative population in NO($v=1$) was greater than that expected by PST.

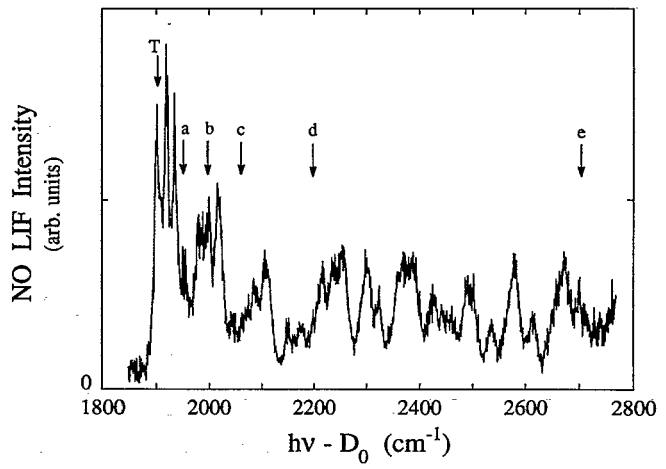

FIG. 3. Photofragment yield spectrum of NO_2 obtained by monitoring NO($X\,^2\Pi_{1/2}$, $v=1$, $J=3.5$). The $R_{11}+Q_{21}(3.5)$ line was monitored as a function of photolysis laser frequency ν. T=thermodynamic threshold for the appearance of NO($v=1$, $J=3.5$; a–e=excess energies where NO product state distributions were measured in this study). $D_0=25\,130.6$ cm^{-1} is the dissociation threshold.

Figures 2 and 3 depict photofragment yield (PHOFRY) spectra obtained by scanning the photolysis laser through the NO(v=0) and NO(v=1) thresholds, respectively, while holding the probe laser frequency fixed to monitor J_{NO}=3.5 in the γ(0,0) and γ(1,1) bands. Photolysis products were always observed at their energetic thresholds, placing an upper limit to dissociation barriers of <2 cm^{-1} (our experimental uncertainty in photolysis energy).[45] The PHOFRY spectra contain a rich structure of irregularly scattered peaks of 5–20 cm^{-1} width, as observed also in the O(^3P_J) PHOFRY spectra obtained in the same energy region by Miyawaki *et al.*,[20] and reproducing the NO(v=0, J_{NO}) yields measured by Robra *et al.* at low $E^\dagger$.[21] By consideration of the density of states around D_0,[20–23] and the degree of lifetime-broadening expected from the measured dissociation rates,[23–25] it is likely that the peaks observed in the PHOFRY spectra reflect the discrete nature of the NO_2 absorption spectrum. However, this interpretation must be treated with caution, since interference effects between overlapping resonances in the decaying NO_2 parent are also expected to result in marked fluctuations in the bandwidths and peak positions.[54] The structures we observe are resolved only at the low NO_2 temperatures achieved in the jet expansion ($T_{rot}<10$ K); at 300 K, the discrete nature of the PHOFRY spectra vanishes.[42]

NO PSDs were obtained from LIF spectra at several excess energies above the NO(v=1) threshold ($E^\dagger$=1949, 1998, 2061, 2200, 2700, and 3038 cm^{-1}, $E_{NO(v=1)}$ = 1876 cm^{-1}). The NO(v=0,1) rotational distributions exhibit sharp fluctuations, which show a marked sensitivity to photolysis energy. However, all distributions contain significant population of *all* energetically allowed J_{NO} rotational levels, and their overall envelopes tend to follow a statistical distribution predicted by PST. The agreement with PST becomes even more pronounced after averaging over the separate Λ-doublet components $\Pi(A'')$ and $\Pi(A')$. [$Q_{11}+P_{21}$ and R_{21} branches probe the $\Pi(A'')$ levels, while the P_{11} and $R_{11}+Q_{21}$ lines probe the $\Pi(A')$ levels in the NO($^2\Pi_{1/2}$) γ bands.] For example, in the NO($^2\Pi_{1/2}$, v=0) rotational distribution obtained at $E^\dagger$=1949 cm^{-1} (Fig. 4), the $\Pi(A')$ levels are consistently less populated than $\Pi(A'')$ levels for $16.5\leqslant J_{NO}\leqslant 20.5$, while the reverse is true for J_{NO}=22.5–23.5. Averaging over the Λ-doublet components, however, brings the distribution in closer agreement with PST. This is particularly evident when the data are displayed in a Boltzmann plot [Fig. 5(a)]. We note that no consistent propensity for a particular Λ-doublet component was observed in our experiments.

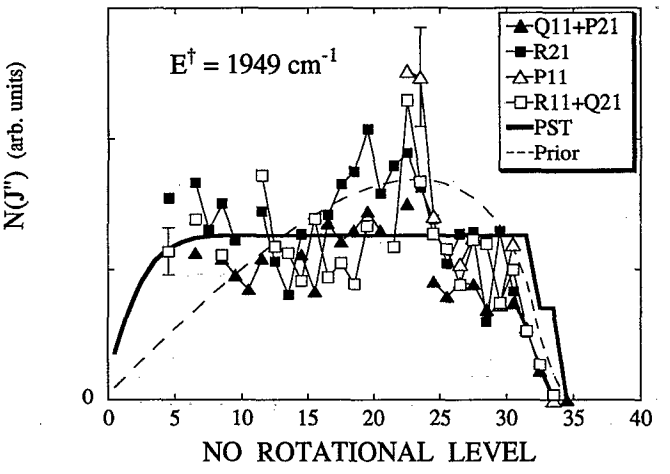

FIG. 4. Rotational level distributions of NO($X\,^2\Pi_{1/2}$, v=0) following dissociation of NO_2 at $E^\dagger$=1949 cm^{-1} (position *a* in Fig. 3). The $Q_{11}+P_{21}$ and R_{21} branches correspond to the $\Pi(A'')$ Λ-doublet component, while the $R_{11}+Q_{21}$ and P_{11} branches correspond to the $\Pi(A')$ component. The results are compared with PST calculations (solid line) and a prior distribution (dashed line).

In all the NO(v=0,1) rotational distributions, the trend to cluster about the expectations of PST is apparent (Figs. 5 and 6). This agreement is particularly good in the NO(v=1) distributions at $E^\dagger<3000$ cm^{-1}, and in some of the NO(v=0) distributions (e.g., at $E^\dagger$=2700 cm^{-1}). However, at other photolysis energies, the deviations from PST are quite severe. This is the case, e.g., in the NO(v=0) distribution at $E^\dagger$=2061 cm^{-1}, where a large, broad maximum is found for J_{NO}=20.5–25.5 (E_{NO}=700–1100 cm^{-1}), or in the NO(v=1) channel at $E^\dagger$=3038 cm^{-1}, where prominent peaks are found at the lower and higher J_{NO}. The prior distributions, on the other hand, underestimate the population of the lower J_{NO} rotational levels at all $E^\dagger$ (see Sec. IV).

In contrast, both PST and prior calculations underestimate the NO vibrational excitations. These are summarized in Table I, in which the separate distributions for each NO spin–orbit state are given, as well as the total vibrational distributions. The total population percentage

TABLE I. NO($X\,^2\Pi_\Omega$; v=0,1) vibrational and spin–orbit distributions from NO_2 photolysis.

$E^\dagger$ (cm^{-1})	%NO(v=0)			%NO(v=1)			%Total(v=0,1)	
	$\Pi_{1/2}$	$\Pi_{3/2}$	Tot	$\Pi_{1/2}$	$\Pi_{3/2}$	Tot	$\Pi_{1/2}$	$\Pi_{3/2}$
392	77.0±11.6	23.0±3.5	100	···	···	···	77.0±11.6	23.0±3.5
1949	50.5±7.6	22.4±3.4	72.9±10.9	27.1±4.1	···	27.1±4.1	77.6±11.6	22.4±3.4
1998	57.2±8.6	22.3±3.3	79.5±11.9	20.2±3.0	0.3±0.05	20.5±3.1	77.4±11.6	22.6±3.4
2061	56.7±8.5	23.3±3.5	80.0±12.0	18.1±2.7	1.9±0.3	20.0±3.0	74.8±11.2	25.2±3.8
2200	39.0±5.9	18.6±2.8	57.6±8.6	34.3±5.1	8.1±1.2	42.4±6.4	73.3±11.0	26.7±4.0
2700	38.1±5.7	18.1±2.7	56.2±8.4	31.8±4.8	12.0±1.8	43.8±6.6	69.9±10.5	30.1±4.5
3038	41.0±6.2	17.8±2.7	58.8±8.8	29.2±4.4	12.0±1.8	41.2±6.2	70.2±10.5	29.8±4.5

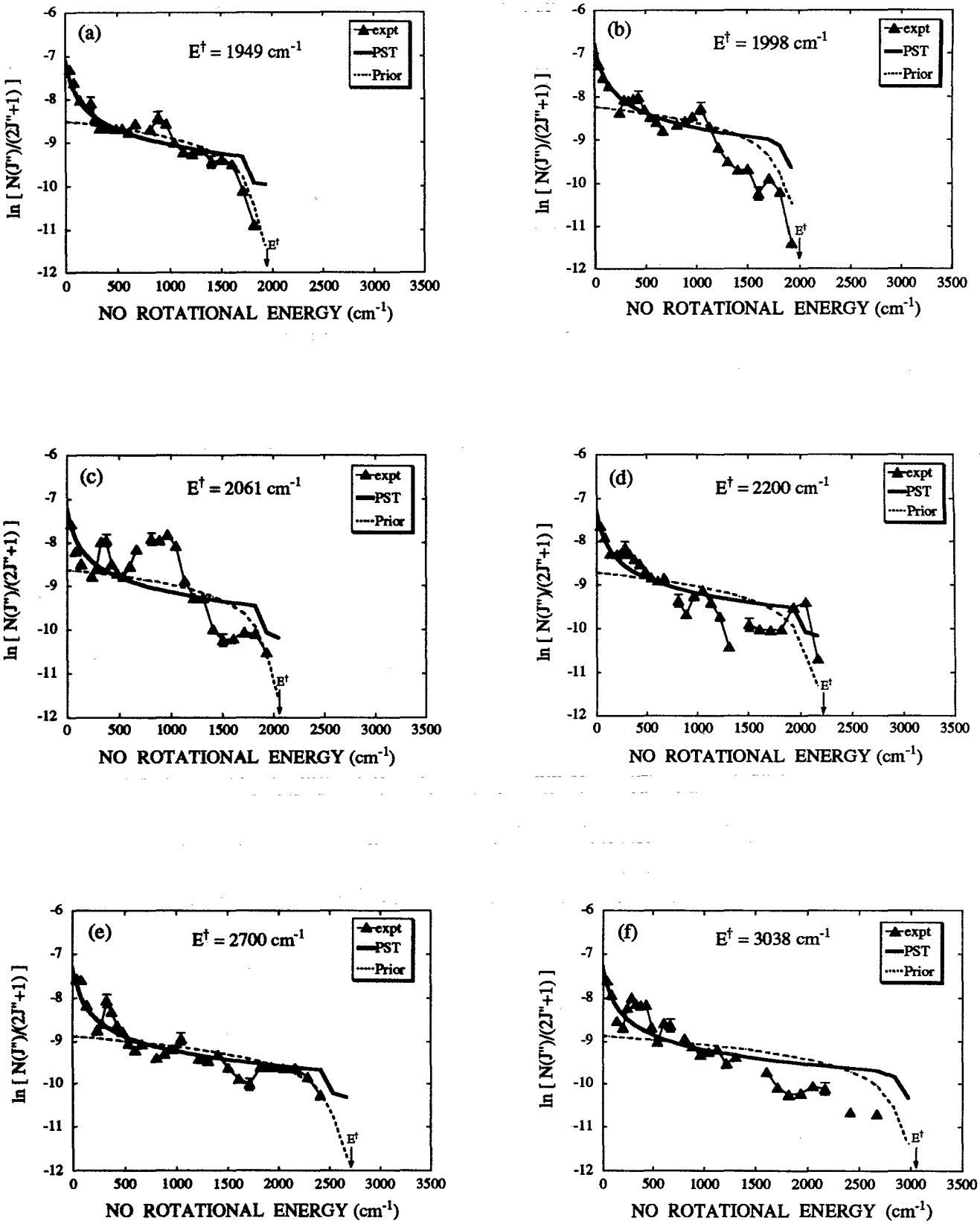

FIG. 5. Boltzmann plots of NO($X\,^2\Pi_{1/2}$, v=0) rotational distributions, averaged over the $\Pi(A')$ and $\Pi(A'')$ Λ-doublet components, obtained from NO_2 photolysis at wavelengths (a) 369.28; (b) 368.61; (c) 367.76; (d) 365.88; (e) 359.31; and (f) 355 nm. The results are compared with PST calculations (solid lines) and prior distributions (dashed lines).

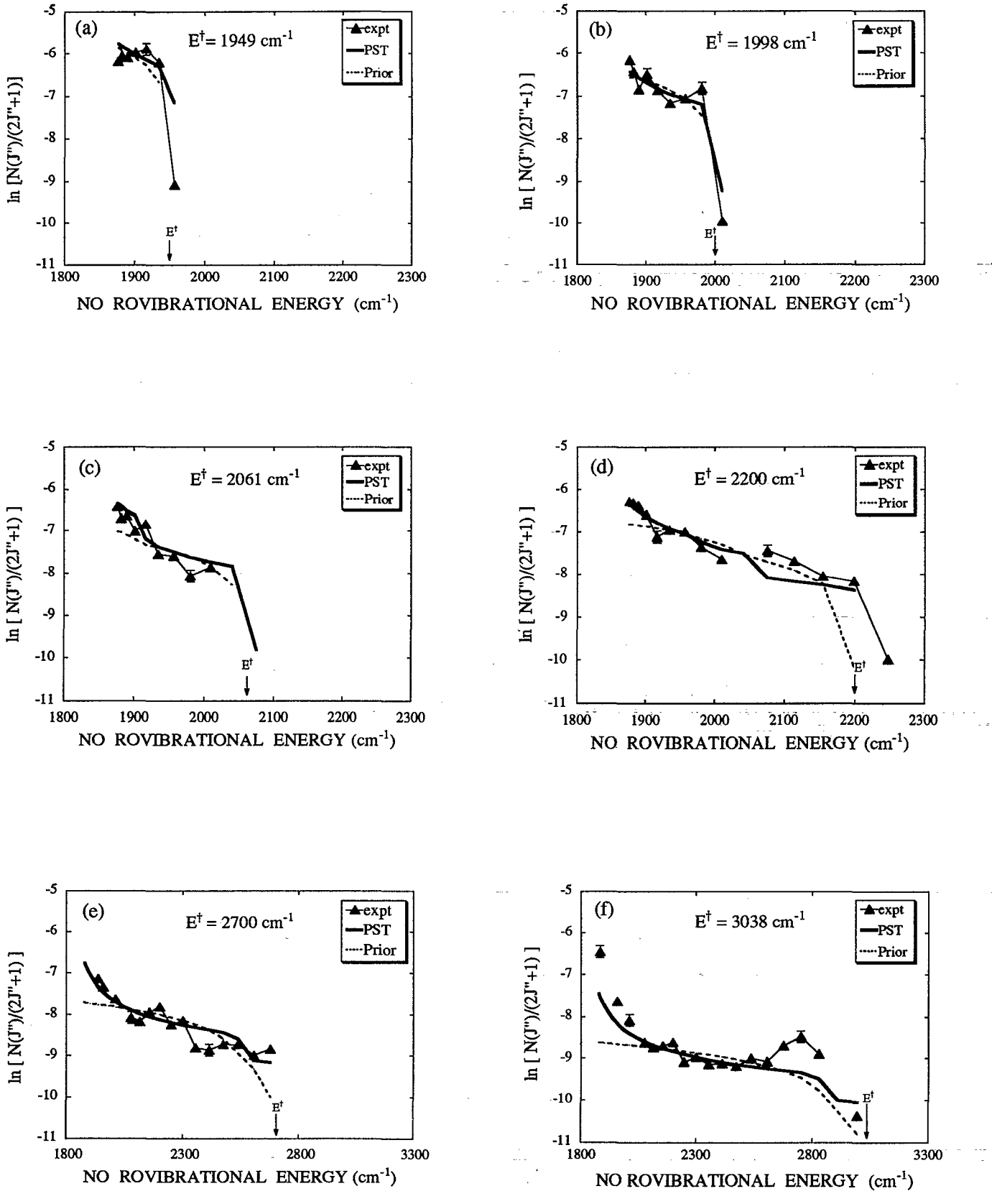

FIG. 6. Boltzmann plots of NO($X\,^2\Pi_{1/2}$, $v=1$) rotational distributions averaged over the $\Pi(A')$ and $\Pi(A'')$ Λ-doublet components obtained from NO_2 photolysis at wavelengths (a) 369.28; (b) 368.61; (c) 367.76; (d) 365.88; (e) 359.31; and (f) 355 nm. The results are compared with PST calculations (solid lines) and prior distributions (dashed lines).

in each NO spin–orbit state for each $E^\dagger$ is given in the last column. Theory and experiment are compared in Fig. 7, where the percent of the total vibrational population in $v=1$ is plotted as a function of $E^\dagger$ and compared with several statistical treatments, which are discussed in Secs. IV and V. Note that Fig. 7 shows a *decrease* in vibrational excitation as the excess energy was increased around $E^\dagger=2000\ cm^{-1}$. This nonmonotonic behavior has been observed also in our preliminary study using REMPI for NO detection, although the larger uncertainty in those data (due to partial saturation of the NO γ bands) had prevented us from stressing it more forcibly.[45] This finding is significant, since all statistical theories predict a monotonic increase of vibrational excitation of NO as a function of excess energy. It is possible, however, that this nonmonotonic behavior derives from fluctuations in the NO rotational distributions that are not averaged even when summing over all the rotational levels to obtain the vibrational populations. These fluctuations in the vibrational distributions should be noticeable particularly near the $v=1$ threshold, where the number of $v=1$ rotational channels is still very small (see Fig. 6). However, other dynamical sources may also cause some of this behavior (*vide infra*).

An interesting point concerns the $NO(^2\Pi_\Omega;\ \Omega=1/2,3/2)$ spin–orbit distributions. These were found to be colder than expected by PST, in both $NO(v=0)$ and $NO(v=1)$ channels. Furthermore, the overall ratio $NO(^2\Pi_{1/2};\ v=0,1)/NO(^2\Pi_{3/2};\ v=0,1)$ varied only slightly with photolysis energy (Table I). This is in sharp contrast to the large fluctuations in the $O(^3P_J)$ spin–orbit ratios observed in the same energy range by Miyawaki *et al.*[20] Equally intriguing is the fact that the rotational distributions with their associated structures in both $NO(v=0)$ and $NO(v=1)$ are independent of the NO product spin–orbit level after averaging over the Λ-doublet components, and an example is shown in Fig. 8.

NO product state distributions were also obtained at $E^\dagger=392\ cm^{-1}$. A prominent peak in the PHOFRY spectra is present in this region (position *a* in Fig. 2), and the $O(^3P_J)$ spin–orbit distribution at this energy had been found previously to be statistical.[20] It was thus of interest to determine whether the NO internal energy states at this photolysis energy would also be populated statistically. Figure 9 shows our observed $NO(^2\Pi_{1/2})$ rotational distribution at $E^\dagger=392\ cm^{-1}$, once again, the average distribution is fairly well described by PST, but the individual $\Pi(A'')$ and $\Pi(A')$ levels show pronounced fluctuations. In addition, the NO spin–orbit distribution is markedly colder than statistical (Table I). Thus, it seems unlikely one could attach any particular significance to the statistical $O(^3P_J)$ spin–orbit ratio observed at this excess energy.

IV. COMPARISONS WITH STATISTICAL THEORIES

In assessing the statistical nature of NO_2 photofragmentation, the measured $NO(v=0,1)$ R and V distributions were compared with PST (and its SSE/PST variant) and with microcanonical prior distributions. These two approaches differ in their basic statistical assumptions[48] and can thus show significant differences in the PSDs they each predict. The differences become particularly noticeable when treating the unimolecular decay of triatomic molecules from well-defined initial energies and angular momentum states, as is the case in the present experiments.

The PST and prior distributions were derived according to well established procedures.[16–18,46–48] The salient features of each approach, and its application to NO_2 photodissociation, are described in the Appendix. Briefly, the principal differences between the models are (i) PST accounts for total angular momentum conservation, whereas

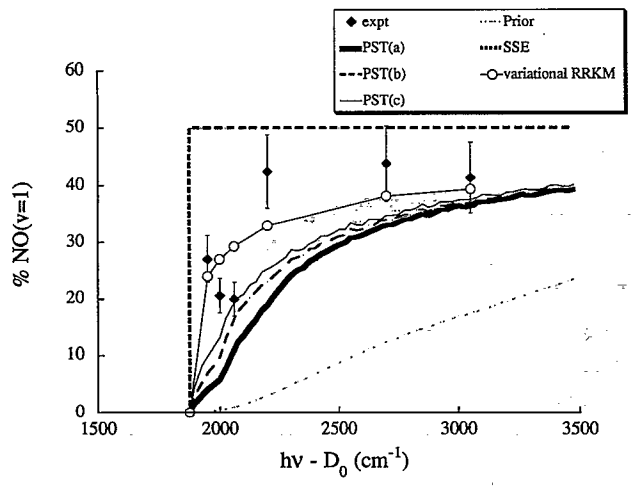

FIG. 7. Measured and calculated $NO(v=1)$ relative populations as a function of $E^\dagger=h\nu-D_0$. The measured distributions are the sums of the separate $^2\Pi_{1/2}$ and $^2\Pi_{3/2}$ NO distributions given in Table I. PST curves were obtained assuming (a) statistical $O(^3P_J)$ and $NO(^2\Pi_\Omega)$ spin–orbit ratios; (b) statistical $NO(^2\Pi_\Omega)$, but 0 K $O(^3P_J)$ spin–orbit distributions; (c) a 2.2:1 $NO(^2\Pi_{1/2}):NO(^2\Pi_{3/2})$ ratio and 0 K $O(^3P_J)$ spin–orbit distribution. Statistical prior expectations, and results of calculations using the SSE method and variational RRKM theory (from Ref. 49), are also shown. See the text for details.

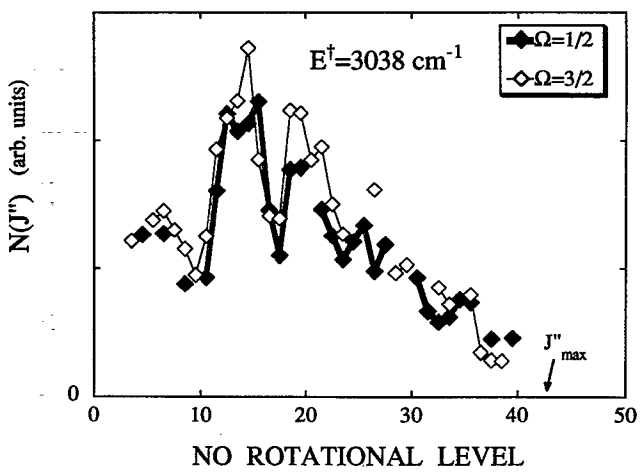

FIG. 8. Separate rotational distributions of $NO(X\ ^2\Pi_{1/2,3/2},\ v=0)$, each averaged over the $\Pi(A')$ and $\Pi(A'')$ Λ-doublet components, following dissociation of NO_2 at $E^\dagger=3038\ cm^{-1}$ (355 nm). The $NO(^2\Pi_{3/2})$ relative populations (empty diamonds) have been arbitrarily scaled for direct comparison with the $NO(^2\Pi_{1/2})$ distribution (filled diamonds) (see Table I).

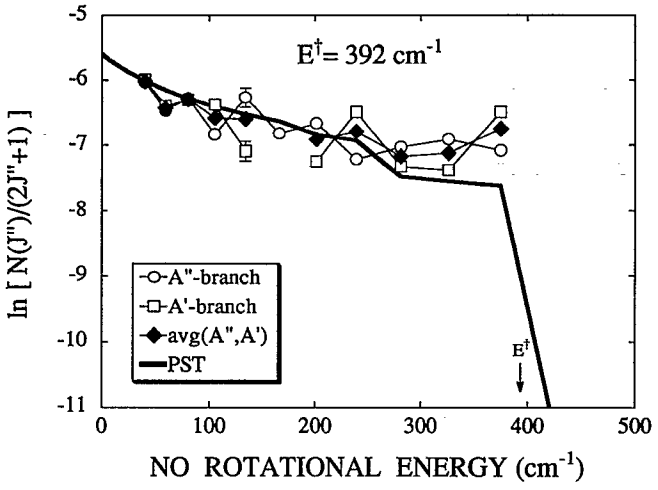

FIG. 9. A Boltzmann plot of the NO($X\,^2\Pi_{1/2}$, $v=0$) rotational distribution obtained from NO_2 photolysis at $E^\dagger=392$ cm^{-1} (position *a* in Fig. 2), and comparison with PST (solid line). Notice that the fluctuations are diminished when the two Λ-doublet components are averaged.

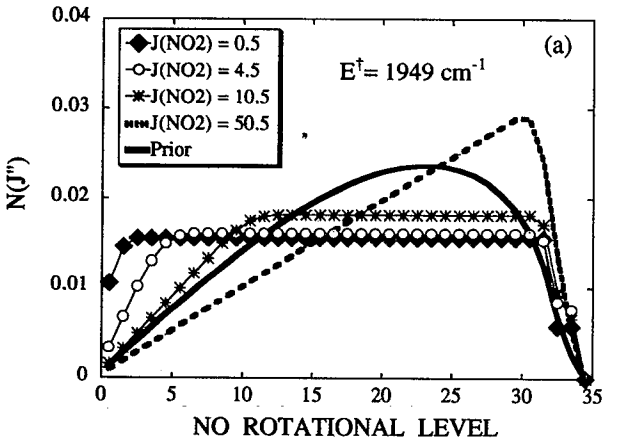

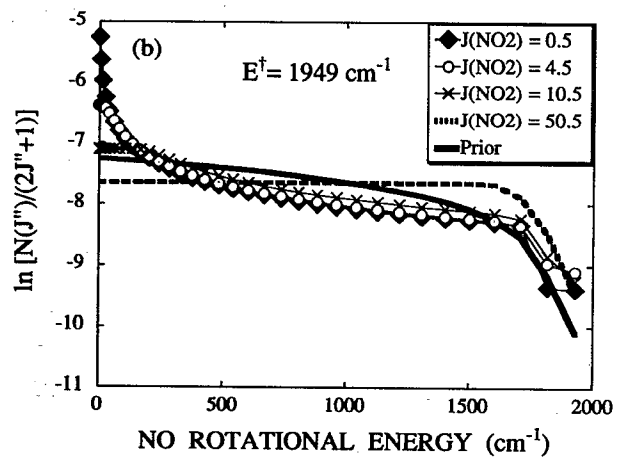

FIG. 10. (a) The effect of NO_2 parent total angular momentum (J_{NO2}) on PST calculations of NO product rotational distributions at $E^\dagger=1949$ cm^{-1}. A prior distribution is included for comparison (solid line). (b) The effect of NO_2 parent total angular momentum (J_{NO2}) on Boltzmann plots of NO product rotational distributions predicted by PST at $E^\dagger=1949$ cm^{-1}. Notice the bimodal distribution at $J_{NO2}<10.5$. A prior distribution is included for comparison (solid line).

prior distributions do not. In addition, PST incorporates dynamical constraints arising from centrifugal barriers in the exit channel; (ii) PST utilizes a flux measure in phase space, whereby each pair of energetically accessible NO($^2\Pi_\Omega$,v_{NO},J_{NO}) and O(^3P_J) product levels is weighted by the product of its density of states and the relative velocity of the NO and O photofragments. Prior distributions, on the other hand, use a uniform measure in which product levels are simply weighted by their densities of states.[48]

These differences between the theories have a pronounced impact in unimolecular reactions where one of the fragments has only a limited range of angular momentum states (e.g., an atom). In particular, the angular momentum constraints included in PST result in a marked dependence of the PSDs on the total angular momentum of the parent molecule. In NO_2 decomposition, e.g., the O(^3P_J) fragment is limited to $J=2$, 1, and 0; consequently, the NO PSDs predicted by PST can differ significantly from prior distributions. The effect on the NO rotational distributions is depicted in Fig. 10(a), where we display PST distributions as a function of NO_2 total angular momentum J_{NO_2} at a fixed excess energy $E^\dagger=1949$ cm^{-1}. For low J_{NO_2}, all NO rotational levels J_{NO} tend to become equally populated, whereas in the high J_{NO_2} limit, the J_{NO} populations predicted by PST become directly proportional to the rotational level degeneracy $(2J_{NO}+1)$. When displayed in a Boltzmann plot, these differences are manifested as a trend for the distributions from low J_{NO_2} to show a "bimodal" character, with a colder component at the lower J_{NO} levels [Fig. 10(b)]. Prior rotational distributions, on the other hand, are independent of J_{NO_2}, and the J_{NO} population is roughly proportional to the NO rotational level degeneracy. Thus, prior distributions are similar to PST calculations only in the high J_{NO_2} limit, and they do not show a bimodal appearance in Boltzmann plots (Fig. 10).

Despite showing significant fluctuations, our measured NO($v=0,1$) rotational distributions are in good agreement with the predictions of PST (Figs. 5 and 6). In particular, the data consistently show the colder component at low J_{NO} as expected by PST. At higher temperatures, however, this colder component should vanish and the distributions become more prior-like. At 300 K, e.g., the average NO_2 total angular momentum is $\langle J_{NO_2}\rangle = 26.5$, and the bimodal behavior disappears (Fig. 11). This accounts for the good agreement with prior distributions obtained in the NO($v=1$) rotational distributions by Mons and Dimicoli using photolysis of 300 K NO_2 samples.[42] However, it is clear that the bimodal distributions obtained from 300 K NO_2 by Welge *et al.*[37] at yet higher excess energies can be reconciled neither with prior distributions nor with PST.

The inclusion of angular momentum constraints in PST also results in a marked sensitivity of the NO($v=0,1$) vibrational populations to J_{NO_2}. This effect is most pronounced at photolysis energies immediately above the threshold for NO($v=1$) production. At these $E^\dagger$, the high-

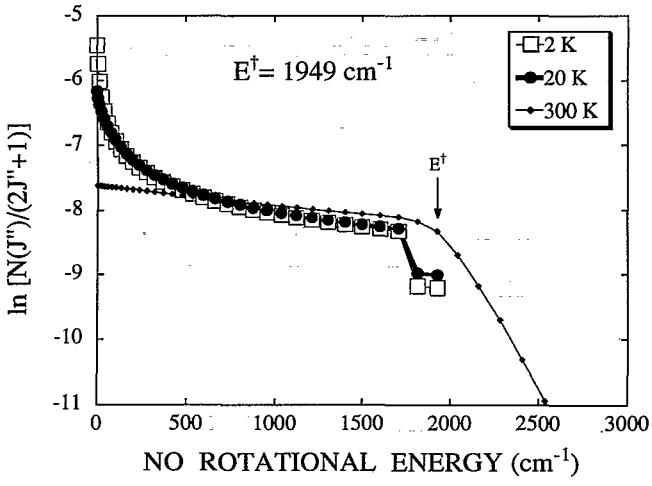

FIG. 11. The effect of NO_2 parent rotational temperature on PST calculations of NO product rotational distributions at $E^\dagger = 1949$ cm^{-1} (Boltzmann plot). The bimodal distribution at <20 K disappears at 300 K.

est NO rotational levels accessible by energy conservation for each vibrational state are $J_{NO}^{max}(v=0;\ E^\dagger) \gg J_{NO}^{max}(v=1;\ E^\dagger)$; consequently, varying J_{NO_2} has a much larger effect on the phase space available to the NO($v=0$) channel than to NO($v=1$). In particular, as $J_{NO_2} \to 0$, the number of accessible (J_{NO}, L) levels in the NO($v=0$) channel is sharply reduced, while the number in the NO($v=1$) channel remains practically unaltered. This is shown schematically in Fig. 12, in which L denotes the relative orbital angular momentum of the NO and O photofragments (see the Appendix). Conversely, as $J_{NO_2} \to \infty$, the phase space available to each J_{NO} level becomes directly proportional to its $(2J_{NO}+1)$ degeneracy, and the relative population in the NO($v=0$) channel accordingly increases. As a result, PST may predict vibrational distributions which are either hotter or colder than prior distributions near the NO($v=1$)

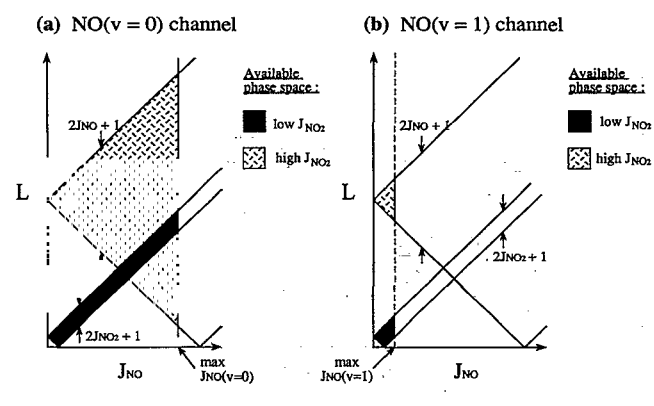

FIG. 12. Diagrammatic representation of the effect of NO_2 parent total angular momentum J_{NO2} on the NO($v=0,1$) product vibrational distributions. L is the relative orbital angular momentum of the NO and O photofragments, and J_{NO} denotes the total angular momentum of the NO product. The two limiting cases of low and high J_{NO2} are depicted for both NO($v=0$) and NO($v=1$) channels [panels (a) and (b), respectively].

TABLE II. Comparison of prior calculations and PST on predicting NO($v=0,1$) relative populations close to the NO($v=1$) threshold.

	%NO($v=1$)			
	PST			
$E^\dagger$ (cm^{-1})	$J_{NO_2}=0.5$	$J_{NO_2}=10.5$	$J_{NO_2}=50.5$	Prior
1920	3.63	1.35	0.014	0.14
2000	5.90	3.09	1.20	0.53
2200	20.53	13.93	6.75	3.16
2500	30.36	26.15	16.00	8.89
3000	36.80	34.55	25.14	17.13

threshold, depending on whether J_{NO_2} is, respectively, low or high (Table II). Our experiment approaches the low J_{NO_2} limit, since only NO_2 levels with $J_{NO_2} \leqslant 8.5$ are significantly populated at $T_{rot}=6$ K, and thus the PST vibrational distributions are accordingly up to two orders of magnitude hotter than the predictions of prior calculations (Fig. 7). We note that varying the NO_2 temperature between 2 and 20 K has a negligible effect on the PST vibrational excitation. The experimental results, however, indicate even greater NO vibrational excitations than predicted by PST.

A subtle point in modeling the NO($v=0,1$) product vibrational distributions concerns their possible correlation with the $O(^3P_J)$ and $NO(^2\Pi_\Omega)$ spin–orbit distributions. The measured $O(^3P_J)$ ratios are colder than statistical, and fluctuate with photolysis energy.[20] In addition, our experiments indicate an almost constant propensity for production of the lower spin–orbit $NO(^2\Pi_{1/2})$ state (Table I). Therefore, we also performed constrained PST calculations in which we weighted the $O(^3P_J)$ and $NO(^2\Pi_\Omega)$ spin–orbit channels in order to match their measured distributions. The NO rotational distributions remained essentially unaffected; however, a significant increase in the degree of vibrational excitation was observed, particularly close to the $v=1$ threshold region $E^\dagger = 1800$–2300 cm^{-1}. The constrained distributions are shown in Fig. 7; curve 7(b) corresponds to the limiting case where only the lowest spin–orbit state $O(^3P_2)$, is populated, whereas curve 7(c) includes the further constraint $NO(^2\Pi_{1/2})/NO(^2\Pi_{3/2}) = 2.2$—the measured NO spin–orbit ratio in this energy region. The increased vibrational excitation observed in the constrained PST curves reflects a proportionately larger reduction in the number of open channels available to NO($v=0$) products than for NO($v=1$). For example, at $E^\dagger = 1876$–2034 cm^{-1}, only the $O(^3P_2)$ channel is open for NO($v=1$), while all three $O(^3P_{2,1,0})$ channels are open for NO($v=0$). Therefore, imposing the constraint that only $O(^3P_2)$ is populated does not affect the number of open channels for NO($v=1$), while the number of available states for NO($v=0$) is reduced by a factor of ~ 2. A similar argument explains the increased vibrational excitation expected when imposing a cold NO spin–orbit distribution [Fig. 7(c)].

A final point about our PST calculations concerns the inclusion of centrifugal barriers (see the Appendix). Their

effect on the PSDs is determined by the long-range attractive potential between the separating fragments, which can be approximated by a Lennard-Jones potential $V_{atn}(r) = -C_6 r^{-6}$ (in our case, r is the distance between the O atom and the NO center of mass). From the known atomic polarizability of $O(^3P)$ and the dipole moment of NO, it is possible to estimate C_6 as 10^{-78} J m^6.[16(a)] However, we found that using this value for C_6 in our PST calculations caused truncation of the NO rotational distributions below the maximum allowed by energy conservation. For example, at $E^\dagger = 1949$ cm^{-1}, $N_{PST}(J_{NO} \geqslant 30.5; C_6 = 10^{-78}$ J m$^6) = 0$, while the highest observed J_{NO} is 34.5 (see Fig. 4). Since our experimental distributions did not show any evidence of truncation at the higher J_{NO} levels, we arbitrarily increased the C_6 value to 10^{-76} J m^6 in order to better reproduce our data. This is consistent with the lack of centrifugal barriers deduced from the PHOFRY spectra (or equivalently, to a long-range attractive potential with a stronger than an r^{-6} dependence).

Our measured vibrational distributions are still hotter than those obtained when using even the constrained PST calculations. However, they do not exhibit a population inversion and may thus be accommodated within the framework of a more restricted statistical theory, such as the SSE/PST variant of PST.[2] The SSE method imposes the restriction that product vibrational excitation is derived from an ensemble that includes only the parent vibrational degrees of freedom. It is based on the physical assumption that product vibrational distributions are established earlier along the reaction coordinate than are R and T distributions and then evolve adiabatically, and that parent rotations are not yet mixed with the vibrational modes. To incorporate this restriction, SSE considers two different ensembles. First, product vibrational distributions are derived from an ensemble of parent vibrational degrees of freedom (i.e., excluding parent rotation). Second, product R and T excitations are obtained, for each set of product vibrational states, from an ensemble that includes (i) only those parent vibrational degrees of freedom which evolve into fragment rotations and translations (i.e., the "transitional" modes), and (ii) the parent rotational degrees of freedom. We also note that SSE apportions the vibrational energy according to a density of states criterion rather than a flux measure of phase space as in PST.

The great advantage of SSE is that it imposes a physical constraint that is rather realistic, without adding to the computational complexity. In other systems where SSE was applied, a very loose, PST-like TS has been assumed, and consequently the transitional low-frequency modes were treated as internal rotors (i.e., each with a density of states proportional to $E^{-1/2}$). In the two cases where comparisons are available, NCNO and CH_2CO, the SSE method gave as good an agreement with the experimental observations as did the much more elaborate variational RRKM calculations.[6(c),8,55,56]

The application of the SSE method to NO_2 decomposition is particularly simple. The transitional modes are the bend and the reaction coordinate, and when assuming a PST-like TS, we obtain trivially that the fractional population of NO($v=1$) is 0.5, independent of $E^\dagger$, from threshold to the opening of the $v=2$ channel (see the Appendix). This is indicated in Fig. 7 as the dashed line at 50% NO($v=1$). However, in some cases, a tighter TS than used in PST may be necessary to describe the vibrational distributions. In such cases, some of the transitional modes should not be treated as free rotors, but rather as low-frequency bends. Wittig and co-workers have recently shown that a TS which is tighter than in PST is needed to describe the decomposition rates of NO_2.[23] Consequently, we also used in the SSE calculations a TS bend frequency of 100 cm^{-1}, which is close to the quantized steps observed in the near-threshold NO_2 rate measurements (see the Appendix).[23] The results of the calculations are compared with the experimental values in Table III, and it is clear that the experimental results are bounded between the predictions of the two SSE models.

TABLE III. Percent population in NO $v=1$.

$E^\dagger$ (cm^{-1})	PST[a]	SSE(1)[b]	SSE(2)[c]	Var. RRKM[d]	Expt.[e]
1949	4	50	13	24	27.1±4.1
1998	5	50	19	27	20.5±3.1
2061	10	50	22	29	20.0±3.0
2200	19	50	26	33	42.4±6.4
2700	33	50	33	38	43.8±6.6
3038	36	50	36	39	41.2±6.2

[a]PST calculations assuming a statistical distribution of NO and O spin–orbit states and a temperature of 10 K.
[b]SSE calculations assuming a free rotor for the TS bend and no product spin–orbit excitation.
[c]SSE calculations assuming 100 cm^{-1} frequency for the TS bend and no product spin–orbit excitation.
[d]Variational RRKM calculations from Ref. 49 assuming no spin–orbit excitation and $J_{NO_2} = 5.5$.
[e]Experimental results.

V. DISCUSSION

The NO($v=0,1$) PSDs obtained from NO_2 photolysis at $E^\dagger = 0$–3038 cm^{-1} have several features characteristic of statistical behavior: (i) the rotational distributions cluster around an average that is fairly well described by PST (despite showing significant fluctuations); (ii) for each $E^\dagger$, all product rotational levels allowed by energy and angular momentum conservation are observed; (iii) the energetic threshold for formation of each product channel agrees with the thermochemical expectations, giving no evidence for barriers to dissociation; and (iv) the vibrational distributions are accommodated within the framework of the SSE method. In addition, time resolved measurements of the decay rates at $E^\dagger = 0$–1500 cm^{-1} can be reconciled with RRKM theory when using experimental densities of states.[23] Nevertheless, the classification of the unimolecular reaction of NO_2 as a statistical process should be scrutinized carefully, in view of the existence of a conical intersection and several dynamical features in the dissociation.

We find that, as in other cases, PST consistently underestimates the degree of vibrational excitation; nevertheless, the vibrational distributions fall within the predictions of a more restrictive statistical theory—the SSE method.

For NO_2 decay at the $E^\dagger$ regions of interest here, it predicts a constant 50% $NO(v=1)$ yield when assuming a PST-like TS, thus providing an upper bound to our results and reproducing them reasonably well at $E^\dagger=2200$–3030 cm^{-1}. SSE calculations employing low bend frequencies at the TS provide a lower bound to the experimental results (Table III) and are rather insensitive to the TS bend frequency in the region 20–100 cm^{-1}. Thus, the SSE method provides a better estimate for the vibrational distributions than does PST, while still not requiring knowledge of the PES as does the variational RRKM theory. We note that because of the existence of fluctuations in the vibrational distributions, a more quantitative comparison is difficult. It is likely that a model incorporating an $E^\dagger$-dependent TS, as in the variational RRKM theory, will provide yet a better description of the vibrational distributions. Such a model, which necessitates knowledge of the PES in the TS region, has been used very recently by Klippenstein and Radivoyevitch. These authors calculated *ab initio* the PES in the TS region (i.e., at O–NO separations of 1.9–3.0 Å), and obtained fair agreement with the experimental results, as can be seen in Fig. 7 and Table III.[49] The variational RRKM theory, like the SSE method, includes dynamical constraints in the form of restrictions on couplings between the parent molecule's degrees of freedom (viz., vibrational and rotational modes). The calculations suggest that the NO vibrations are fixed near the TS that also controls the dissociation rates, which is tighter than the one assumed in PST, and from then on they evolve adiabatically.[49]

It is less likely, however, that the $NO(^2\Pi_\Omega)$ and $O(^3P_J)$ spin–orbit distributions could be accounted for without knowledge of the full PES. Unlike the $NO(v=0,1)$ R and V distributions, the product electronic degrees of freedom appear to be determined by dynamical biases; their cold populations, and the sharp fluctuations observed in the $O(^3P_J)$ ratios as a function of $E^\dagger$, probably reflect the persistence of long-range interactions between the NO and O fragments long after the NO product vibrational and rotational distributions have been established. This interpretation is supported by the observation of nearly equal structures and fluctuations in the rotational distributions obtained for the two NO spin–orbit states at each $E^\dagger$ (e.g., Fig. 8).

Adding to this complexity are the marked fluctuations that are a persistent feature of the PSDs in the photolysis of expansion-cooled NO_2. Miyawaki *et al.* have observed them in the $O(^3P_J)$ ratios for $E^\dagger<2200$ cm^{-1},[20] and we detect significant structures in $NO(v=0,1)$ rotational distributions at all $E^\dagger<3100$ cm^{-1} and in the vibrational distributions near the $v=1$ threshold. As proposed in our preliminary communication,[45] these fluctuations may arise from interference effects inherent in the unimolecular decay of a system with overlapping resonances (i.e., Ericson fluctuations, as observed in nuclear reaction cross sections).[54,57–59] The nature of Ericson fluctuations is such that in the limit of a large number of overlapping resonances, they are not expected to vanish; rather, they become increasingly random and hence more tractable by statistical methods. They would not be discernible, however, if the initial state preparation was not selective, or if a large number of product channels is available, in which case, these fluctuations would tend to average out. The latter restrictions are overcome in our experiments by the narrow range of NO_2 initial states obtained in our jet-cooled samples and by the limited number of $O(^3P_J)$ product channels. Furthermore, from consideration of the NO_2 density of states[20–23] and dissociation lifetimes[23–25] in our photolysis region, one would expect excitation of several overlapping resonances following laser excitation from a single rotational level of the ground state. Thus, it is plausible that Ericson fluctuations could account for the existence of the marked structures in our NO rotational distributions, which are nevertheless well described on average by PST. We stress, however, that several other factors may also contribute to create these fluctuations, such as non-uniformities in the state-to-state decay rates from single NO_2 resonances, and dynamical effects induced by the $1\,^2B_2/X\,^2A_1$ conical intersection. A closer examination of these fluctuations and their possible interpretations will be presented in a forthcoming publication.[60] We note that similar trends have been observed in the $CO(v=0,1)$ R and V distributions from photolysis of cold CO_2 ($T_{rot}<20$ K) at 157 nm near the threshold for $CO(X\,^1\Sigma^+)+O(^1D)$ production, namely, CO rotational distributions which fluctuate closely about a PST average with a bimodal appearance in the Boltzmann plots.[45,61]

At $E^\dagger>3300$ cm^{-1}, other workers have suggested that the NO PSDs from NO_2 photolysis are nonstatistical, even for 300 K samples; vibrational distributions become inverted, rotational distributions have a bimodal character that cannot be reconciled with PST and the $NO(^2\Pi_\Omega)$ spin–orbit distributions are still colder than statistical.[37] Our results at $E^\dagger<3100$ cm^{-1}, however, do not indicate a clear transition from statistical behavior at lower $E^\dagger$ to the dynamical regime observed at $E^\dagger>3300$ cm^{-1}. Rather, the $NO(v=0,1)$ rotational distributions are on the average well characterized by PST at all $E^\dagger$, but from the onset, they show significant fluctuations which are signatures of the underlying dynamics. The vibrational distributions need to be accounted for by more restrictive statistical theories (e.g., the SSE method, variational RRKM), and they also show some fluctuations. In addition, a marked propensity for production of the lowest NO spin–orbit level $^2\Pi_{1/2}$—which cannot be explained by statistical theories—is always observed.

However, the strong tendency towards statistical behavior is remarkable, given the sparse density of states of NO_2 and the very fast dissociation rates expected in the $E^\dagger$ region studied in this work. At $E^\dagger=700$ cm^{-1}, e.g., the lifetime is <1 ps,[23] and at $E^\dagger=3038$ cm^{-1}, the recoil anisotropy parameter is already 1.4, corresponding to a dissociation time much shorter than a rotational period.[62] We believe that the bulk of the evidence to date indicates that NO_2 decomposition at low $E^\dagger$ can be described as vibrational predissociation from highly mixed levels of predominantly ground state character. Within this statistical framework, our results also suggest that a single TS is not sufficient to describe the energy disposal in NO_2, as well as

in other simple bond-fission reactions. Rather, it appears that in NO_2, the vibrations become adiabatic before the R and T distributions are fixed, and that the nuclear degrees of freedom, in turn, become adiabatic before the NO and O spin–orbit states are determined. Such behavior is also suggested by the experimental and theoretical results on the decay of NCNO and CH_2O, where the R and T excitations are well described by PST—thus exhibiting a very loose TS—while product vibrational distributions are more sensitive to the details of the PES treated with modified statistical theories. We note that marked deviations from PST in the R and T distributions can be observed in simple bond-fission reactions when small barriers in the exit-channel exist, such as in the decay of triplet CH_2CO (Ref. 63) and triplet t-BuNO.[64] Therefore, the close agreement of our observed NO(v=0,1) rotational distributions with PST further indicates that exit-channel barriers are not playing a significant role in NO_2 unimolecular decay at low temperatures and $E^\dagger$.

VI. SUMMARY AND CONCLUSIONS

We have obtained NO(v=0,1) PSDs from the photolysis of expansion-cooled NO_2 ($T_{rot}<10$ K) in the range $E^\dagger$=0–3000 cm^{-1}. Our results show considerable agreement with statistical theories, despite the sparse density of states and short dissociation lifetimes of NO_2. In particular, the NO rotational distributions are well described on average by PST, while the NO(v=1) vibrational populations—albeit higher than expected by PST—are close to the predictions of the SSE method, and are well described by the more elaborate variational RRKM theory. We find that prior distributions cannot reproduce our observed NO PSDs, primarily as a result of neglecting total angular momentum conservation constraints in the dissociation. These constraints are shown to assume particular importance in unimolecular reactions at low temperatures and when one of the fragments is an atom, in which case, PST more adequately describes the PSDs. We note that NO_2 with its small number of degrees of freedom provides an excellent test case for statistical theories, since the differences between the models are quite large. This is particularly evident when comparing the vibrational distributions predicted by the various models (Fig. 7 and Table III).

On the other hand, a significant interplay between dynamical biases and statistical expectations in this unimolecular reaction is revealed as a result of the low temperature of the parent NO_2 and the limited number of product final states. The NO(v=0,1) R and V distributions show marked fluctuations, and the NO($^2\Pi_\Omega$) spin–orbit ratios are consistently colder than statistical. The dynamical features result from effects such as interference among overlapping resonances causing fluctuations, and possible biases imposed by the conical intersection. The relatively good agreement with statistical models for NO_2 decay at $E^\dagger<3000$ cm^{-1} is interpreted as evidence for a vibrational predissociation mechanism involving highly mixed vibronic levels of predominantly ground state character. Such high degree of vibrational mixing in a triatomic molecule is facilitated by the strong conical intersection between the optically accessible $1\,^2B_2$ and the ground $\tilde{X}\,^2A_1$ states.

Although our results show that the salient features of NO_2 decomposition can be reconciled within the framework of statistical theories, more work is necessary in order to understand the dynamical features. Experimental work on the fluctuations and the importance of parent rotation is in progress in our lab using double-resonance excitation schemes. The determination of PSDs at higher $E^\dagger$ using expansion-cooled samples is desirable, since it may show a clearer transition to a dynamical regime. Theoretical work is also needed, both in developing the statistical framework required to fully model the dissociation and in incorporating the effects of the conical intersection. The latter has been found recently to influence the rotational distributions in the $H+H_2$ system,[65] but its effect on the unimolecular reaction of NO_2 is unknown at present.

ACKNOWLEDGMENTS

We wish to thank Craig Bieler for his assistance in analyzing the distributions, C. Wittig, J. Troe, H. Taylor, and S. Ionov for many helpful discussions, and S. Klippenstein and A. Kuppermann for preprints of Refs. 49 and 65. Support by NSF and ARO is gratefully acknowledged.

APPENDIX

1. Prior distributions

Microcanonical prior calculations, which consider an ensemble of NO_2 parent molecules at a fixed total energy, assume that the energy levels of the NO and O products are populated according to their volume in phase space, i.e., that their relative populations, at a given $E^\dagger$, are proportional to their *total density of states* $\rho(v_{NO},J_{NO},J_{O(^3P)};E^\dagger)$.[46–48] Thus, each energetically accessible pair of NO($^2\Pi_\Omega$,v_{NO},J_{NO}) and O(^3P_J) product levels is weighted by the rovibronic and electronic degeneracies of the NO and O fragments, respectively. In addition, the product levels must be weighted by their translational density of states $\rho(E_t)$, where E_t is the relative translational energy of the separating fragments. Since E_t describes motion in three dimensions, $\rho(E_t)\propto E_t^{1/2}$. The microcanonical prior distribution N_{Prior} is thus of the form

$$N_{Prior}(v_{NO},J_{NO},J_{O(^3P)};E^\dagger)\propto\rho(v_{NO},J_{NO},J_{O(^3P)};E^\dagger), \tag{A1}$$

where

$$\rho(v_{NO},J_{NO},J_{O(^3P)};E^\dagger)=(2J_{NO}+1)(2J_{O(^3P)}+1)\times(E_t)^{1/2}, \tag{A2}$$

and energy conservation implies that

$$E_{NO_2}+E^\dagger=E_t+E_{NO}+E_{O(^3P)}. \tag{A3}$$

E_{NO_2}, E_{NO}, and $E_{O(^3P)}$ are the internal energies of each species. No explicit account is taken of total angular momentum conservation nor of any possible centrifugal barrier constraints.

A typical prior NO product rotational distribution increases monotonically with J_{NO}, but shows a gradual truncation at higher J_{NO} as a result of the vanishing translational density of states for the slower photofragments (Fig. 4). In a Boltzmann plot, these distributions have a slight curvature, but may nevertheless be assigned an approximate temperature (Fig. 5).

2. Phase space theory (PST)

PST imposes the conservation of total angular momentum as well as that of total energy

$$\mathbf{J}_{NO_2}=\mathbf{J}_{NO}+\mathbf{J}_{O(^3P)}+\mathbf{L}, \tag{A4}$$

where $\mathbf{J}_{NO_2}$, $\mathbf{J}_{NO}$, and $\mathbf{J}_{O(^3P)}$ are the total angular momenta of each species, and $\mathbf{L}$ is the relative orbital angular momentum of the photofragments.[16–18] Energy conservation imposes an upper limit L_{max} on L, but additional dynamical constraints (e.g., centrifugal barriers) can be added as well. For example, the functional dependence of L_{max} on $E^\dagger$ can be determined by the long-range attractive potential of the dissociating fragments. Utilizing a $V(r)=-C_6r^{-6}$ potential, where C_6 is a constant, L becomes constrained by

$$L(L+1)h^2\leqslant 24\pi^2\mu C_0^{1/3}(E_t/2)^{2/3}, \tag{A5}$$

where μ is the reduced mass of the photofragments and r the distance from the O atom to the NO center of mass.

In PST, unlike in microcanonical prior distributions, the corresponding measure of the phase space available to each product channel is the radial *flux* along the reaction coordinate, i.e., the product of the density of states for that channel and the relative radial velocity of the dissociating fragments.[16–18,48] Thus, the PST distributions N_{PST} for NO_2 decay are given by

$$N_{PST}(v_{NO},J_{NO},J_{O(^3P)},L;E_t,J_{NO_2})$$

$$\propto v_r\rho(v_{NO},J_{NO},J_{O(^3P)},L;E_t,J_{NO_2}), \tag{A6}$$

where

$$v_r=\frac{dr}{dt}=\left(\frac{2E_t}{\mu}\right)^{1/2}, \tag{A7}$$

$$\rho(v_{NO},J_{NO},J_{O(^3P)},L;E_t,J_{NO_2})$$

$$=\rho(E_t)\rho_{int}(v_{NO},J_{NO},J_{O(^3P)},L;J_{NO_2},J'), \tag{A8}$$

$$\rho(E_t)\propto E_t^{1/2}, \tag{A9}$$

$$\rho_{int}(v_{NO},J_{NO},J_{O(^3P)},L,J',J_{NO_2})=\text{constant}\equiv 1, \tag{A10}$$

and $\mathbf{J}'=\mathbf{J}_{NO}+\mathbf{L}$ is constrained by angular momentum conservation to the range

$$|\mathbf{J}_{NO_2}-\mathbf{J}_{O(^3P)}|\leqslant J'\leqslant J_{NO_2}+J_{O(^3P)}. \tag{A11}$$

The need for a different measure of the available phase space arises from the requirement that PST, in which both *E and* J_{NO_2} are conserved, satisfy the principle of detailed balance.[16–18,48] It is important to note that PST considers explicitly only a *radial* translational density of states of the photofragments {hence, a *one*-dimensional density, $\rho(E_t)\propto E_t^{-1/2}$ [Eq. (A9)]}, the other two translational degrees of freedom of the fragments are implicitly accounted for via the L and m_L orbital quantum numbers.[48] Since the radial velocity of the fragments is in turn proportional to $E_t^{1/2}$ [Eq. (A7)], the overall radial flux along the reaction coordinate becomes independent of E_t. Pechukas and Light have shown that, in this case, the simplest statistical assumption that satisfies detailed balance is Eq. (A10), which assigns equal probability to all product channels $(v_{NO},J_{NO},J_{O(^3P)},L;J_{NO_2},J')$ satisfying total energy and angular momentum conservation.[16,17] Combining (A3)–(A11), the final expression for the (unnormalized) PST distributions for NO_2 dissociation becomes

$$N_{PST}(v_{NO},J_{NO},J_{O(^3P)};J_{NO_2},E_t)$$

$$\propto \sum_{J'=|\mathbf{J}_{NO_2}-\mathbf{J}_{O(^3P)}|}^{J_{NO_2}+J_{O(^3P)}} \sum_{J_{NO}=0.5}^{J_{NO}^{max}(E^\dagger,J',v_{NO})} \sum_{L=|\mathbf{J}',\mathbf{J}_{NO}|}^{\substack{L\leqslant J'+J_{NO};\\ L\leqslant L_{max}(E^\dagger,J',v_{NO})}} 1, \tag{A12}$$

where $J_{NO}^{max}(E^\dagger,J',v_{NO})$ is the limit set on J_{NO} by the conservation of energy.

It is worth noting that the $(2J_i+1)$ degeneracies $(i=\text{NO, O})$, which were explicitly included in the N_{Prior} distribution [Eq. (A1)], are implicit in the expression for N_{PST} [Eq. (A12)]. Angular momentum conservation constraints, however, can effectively reduce these degeneracies, particularly as $J_{NO_2}\rightarrow 0$.[16–18,48] This is evident when we write Eq. (A12) in closed form

$$N_{PST}(J_{NO},J_{O(^3P)};J_{NO_2},E^\dagger)\propto \sum_{J'}(2J_a^<+1)(2J_b^<+1), \tag{A13}$$

where J' is given by Eq. (A11), and

$$J_a^<=\begin{cases}J_{O(^3P)};J_{O(^3P)}\leqslant J_{NO_2}\\ J_{NO_2};J_{O(^3P)}\geqslant J_{NO_2}\end{cases}, \tag{A13a}$$

$$J_b^<=\begin{cases}J_{NO};J_{NO}\leqslant J'\\ J';J_{NO}\geqslant J'\end{cases}. \tag{A13b}$$

These constraints result in a marked sensitivity of N_{PST} to the parent angular momentum J_{NO_2} and, consequently, to the temperature of the parent molecule. For this reason, we observe sharp deviations between PST and prior calculations in the PSDs from photodissociation of cold NO_2 ($T_{rot}<10$ K). At 300 K, these differences are expected to become negligible.

3. The SSE method

PST usually underestimates product vibrational excitations, while SSE, which uses a contracted phase space, gives higher vibrational excitations. In the case of a PST-like TS, the fractional NO vibrational population $N_{SSE}(v)$

is proportional to the density of states of an ensemble of T transitional modes, which are treated as T one-dimensional oscillators[2]

$$N_{SSE}(v)=(E^{\dagger}-E_v)^{(0.5T-1)}/\sum(E^{\dagger}-Ev)^{(0.5T-1)}, \tag{A14}$$

where $E^{\dagger}-E_v$ is the energy available in excess of that required to form NO in vibrational state v and the summation is over the allowed NO vibrational levels. In the case of NO_2, $T=2$ since there are two transitional modes, the reaction coordinate (i.e., the asymmetric stretch) and the NO_2 bend. Thus $N_{SSE}(v)=1/(v_{max}+1)$ (where v_{max} is the highest NO vibrational level allowed by energy conservation), yielding 0.5 and 0.33 as the fractional populations of $v=1$ below the thermochemical thresholds for $v=2$ and $v=3$, respectively.

If the NO_2 bend at the TS is treated as a low frequency vibration, as suggested by the near-threshold decomposition rate measurements,[23] the NO(v) fractional population can be calculated by summing explicitly over the allowed bending levels. For example, $N_{SSE}(v=1)$ is given by

$$N_{SSE}(v=1)=\sum(E^{\dagger}-E_{v=1})^{-1/2}\Big/\Big[\sum(E^{\dagger})^{-1/2}+\sum(E^{\dagger}-E_{v=1})^{-1/2}\Big], \tag{A15}$$

where the sum is over the TS bending levels.

[1] H. Reisler and C. Wittig, Annu. Rev. Phys. Chem. **37**, 307 (1986), and references therein.

[2] C. Wittig, I. Nadler, H. Reisler, M. Noble, J. Catanzarite, and G. Radhakrishnan, J. Chem. Phys. **83**, 5581 (1985).

[3] C. X. W. Qian, A. Ogai, H. Reisler, and C. Wittig, J. Chem. Phys. **90**, 209 (1989).

[4] L. R. Khundar, J. L. Knee, and A. H. Zewail, J. Chem. Phys. **87**, 77 (1987).

[5] W. H. Green, Jr., C. B. Moore, and W. F. Polik, Annu. Rev. Phys. Chem. **43**, 591 (1992), and references therein.

[6] (a) I-C. Chen, W. H. Green, and C. B. Moore, J. Chem. Phys. **89**, 314 (1988); (b) W. H. Green, I-C. Chen, and C. B. Moore, Ber. Bunsenges. Phys. Chem. **92**, 389 (1988); (c) W. H. Green, A. J. Mahoney, Q.-K. Zheng, and C. B. Moore, J. Chem. Phys. **94**, 1961 (1991).

[7] B. Schramm, D. J. Bamford, and C. B. Moore, Chem. Phys. Lett. **98**, 305 (1983).

[8] S. K. Kim, Y. S. Choi, C. D. Pibel, Q.-K. Zheng, and C. B. Moore, J. Chem. Phys. **94**, 1954 (1991).

[9] E. D. Potter, M. Gruebele, L. R. Khundar, and A. H. Zewail, Chem. Phys. Lett. **164**, 463 (1989).

[10] F. F. Crim, Annu. Rev. Phys. Chem. **35**, 657 (1984), and references therein.

[11] (a) H.-R. Dubal and F. F. Crim, J. Chem. Phys. **83**, 3863 (1985); (b) T. M. Tichich, T. R. Rizzo, H.-R. Dubal, and F. F. Crim, *ibid.* **84**, 1508 (1986); (c) L. J. Butler, T. M. Tichich, M. D. Likar, and F. F. Crim, *ibid.* **85**, 2331 (1986); (d) T. M. Tichich, M. D. Likar, H.-R. Dubal, L. J. Butler, and F. F. Crim. *ibid.* **87**, 5820 (1987).

[12] L. Brouwer, C. J. Cobos, J. Troe, H. -R. Dubal, and F. F. Crim, J. Chem. Phys. **86**, 6171 (1987).

[13] T. R. Rizzo, C. C. Hayden, and F. F. Crim, Faraday Discuss. Chem. Soc. **75**, 276 (1983).

[14] N. F. Scherer and A. H. Zewail, J. Chem. Phys. **87**, 97 (1987).

[15] (a) X. Luo and T. R. Rizzo, J. Chem. Phys. **93**, 8620 (1990); (b) X. Luo, P. R. Fleming, T. A. Seckel, and T. R. Rizzo, *ibid.* **93**, 9194 (1990).

[16] (a) P. Pechukas, J. C. Light, and C. Rankin, J. Chem. Phys. **44**, 794 (1966); (b) P. Pechukas and J. C. Light, *ibid.* **42**, 3281 (1965).

[17] J. C. Light, Discuss. Faraday Soc. **44**, 14 (1967).

[18] (a) C. E. Klotz, J. Phys. Chem. **75**, 1526 (1971); (b) Z. Naturforsch. Teil A **27**, 553 (1972).

[19] (a) D. M. Wardlaw and R. A. Marcus, Adv. Chem. Phys. **70**, 231 (1988); (b) R. A. Marcus, Philos. Trans. R. Soc. London Ser. A **332**, 283 (1990), and references therein.

[20] (a) J. Miyawaki, K. Yamanouchi, and S. Tsuchiya, Chem. Phys. Lett. **180**, 287 (1991); (b) J. Miyawaki, T. Tsuchizawa, K. Yamanouchi, and S. Tsuchiya, *ibid.* **165**, 168 (1990).

[21] (a) U. Robra, H. Zacharias, and K. H. Welge, Z. Phys. D **16**, 175 (1990); (b) U. Robra, Ph. D. thesis, University of Bielefeld, 1984.

[22] (a) A. Delon and R. Jost, J. Chem. Phys. **95**, 5686 (1991); (b) A. Delon, R. Jost, and M. Lombardi, *ibid.* **95**, 5700 (1991).

[23] (a) G. A. Brucker, S. I. Ionov, Y. Chen, and C. Wittig, Chem. Phys. Lett. **194**, 301 (1992); (b) S. I. Ionov, G. A. Brucker, C. Jaques, Y. Chen, and C. Wittig (to be published).

[24] (a) H. Gaedtke and J. Troe, Ber. Bunsenges. Phys. Chem. **79**, 184 (1975); (b) M. Quack and J. Troe, *ibid.* **79**, 469 (1975); (c) H. Gaedtke, H. Hippler, and J. Troe, Chem. Phys. Lett. **16**, 177 (1972).

[25] E. A. Rohlfing and J. J. Valentini, J. Chem. Phys. **83**, 521 (1985).

[26] (a) A. E. Douglas and K. P. Huber, Can. J. Phys. **43**, 74 (1965); (b) A. E. Douglas, J. Chem. Phys. **45**, 1007 (1966).

[27] R. E. Smalley, L. Wharton, and D. H. Levy, J. Chem. Phys. **63**, 4989 (1976).

[28] (a) C. F. Jackels and E. R. Davidson, J. Chem. Phys. **64**, 2908 (1976); (b) **65**, 2941 (1976).

[29] (a) L. Burnelle, A. M. May, and R. A. Gangi, J. Chem. Phys. **49**, 561 (1968); (b) R. A. Gangi and L. Burnelle, *ibid.* **55**, 851 (1971).

[30] (a) G. D. Gillespie and A. U. Khan, J. Chem. Phys. **65**, 1624 (1976); (b) G. D. Gillespie, A. U. Kahn, A. C. Wahl, R. P. Hosteny, and M. Krauss, *ibid.* **63**, 3425 (1975).

[31] D. Hsu, D. L. Monts, and R. N. Zare, *Spectral Atlas of Nitrogen Dioxide 5530 to 6480 Å* (Academic, New York, 1978).

[32] (a) H. Köppel, W. Domcke, and L. S. Cederbaum, Adv. Chem. Phys. **57**, 59 (1984); (b) E. Haller, H. Köppel, and L. S. Cederbaum, J. Mol. Spectrosc. **111**, 377 (1985); (c) Th. Zimmerman, H. Köppel, and L. S. Cederbaum, J. Chem. Phys. **91**, 3934 (1989).

[33] (a) G. Hirsch and R. J. Buenker, Can. J. Chem. **63**, 1542 (1985); (b) G. Hirsch, R. J. Buenker, and C. Petrangolo, Mol. Phys. **70**, 835 (1990).

[34] (a) K. Shibuya, T. Kusumoto, K. Shibuya, and K. Obi, J. Chem. Phys. **95**, 720 (1991); (b) H. Nagai, K. Aoki, T. Kusumoto, K. Shibuya, and K. Obi, J. Phys. Chem. **95**, 2718 (1991); (c) S. Hiraoka, K. Shibuya, and K. Obi, J. Mol. Spectrosc. **126**, 427 (1987).

[35] R. Jost (private communication).

[36] G. E. Busch and K. R. Wilson, J. Chem. Phys. **56**, 3626 (1972); **56**, 3638 (1972).

[37] (a) H. Zacharias, M. Geilhaupt, K. Meier, and K. H. Welge, J. Chem. Phys. **74**, 218 (1981); (b) H. Zacharias, K. Meier, and K. H. Welge, in *Energy Storage and Redistribution in Molecules*, edited by J. Hinze (Plenum, New York, 1983), p. 107.

[38] (a) K. H. Welge, in *NATO ASI Series B (Physics)* edited by K. L. Kompa and J. Wanner (Plenum, New York, 1984, Vol. 105, p. 123); (b) U. Robra, K. Meier, H. Zacharias, and K. H. Welge, in *Lasers as Reactants and Probes in Chemistry*, edited by W. M. Jackson and A. B. Harvey (Howard University, Washington D.C., 1984), p. 193.

[39] M. Kawasaki, H. Sato, A. Fukuroda, T. Kikuchi, S. Kobayashi, and T. Arikawa, J. Chem. Phys. **86**, 4431 (1987).

[40] K. Chen and C. Pei, Chem. Phys. Lett. **137**, 361 (1987).

[41] H.-G. Rubahn, W. J. van der Zande, R. Zhang, M. J. Bronikowski, and R. N. Zare, Chem. Phys. Lett. **186**, 154 (1991).

[42] (a) M. Mons and I. Dimicoli, Chem. Phys. **130**, 307 (1989); (b) Chem. Phys. Lett. **131**, 298 (1986).

[43] P.-A. Elofson and E. Ljungstrom, Chem. Phys. **165**, 323 (1992).

[44] C. H. Chen, D. W. Clark, M. G. Payne, and S. D. Kramer, Opt. Commun. **32**, 391 (1980).

[45] D. C. Robie, M. Hunter, J. L. Bates, and H. Reisler, Chem. Phys. Lett. **193**, 413 (1992).

[46] J. L. Kinsey, J. Chem. Phys. **54**, 1206 (1971).

[47] (a) R. D. Levine and R. B. Bernstein, Acc. Chem. Res. **7**, 393 (1974); (b) R. D. Levine and J. L. Kinsey, in *Atom–Molecule Collision Theory—A Guide for the Experimentalist*, edited by R. B. Bernstein (Plenum, New York, 1979), Chap. 22; (c) R. D. Levine, in *Photoselective Chemistry*, edited by J. Jortner, R. D. Levine, and S. A. Rice

(Wiley, New York, 1981), p. 239; (d) R. B. Bernstein and R. D. Levine, Adv. At. Mol. Phys. **2**, 45 (1975).
[48] A. Ben-Shaul, Chem. Phys. **22**, 341 (1977).
[49] S. Klippenstein and T. Radivoyevitch (to be published).
[50] C. X. W. Qian, A. Ogai, L. Iwata, and H. Reisler, J. Chem. Phys. **92**, 4296 (1990).
[51] R. J. S. Morrison and E. R. Grant, J. Chem. Phys. **77**, 5994 (1982).
[52] (a) D. C. Jain and R. C. Sahni, Trans. Faraday Soc. **64**, 3169 (1968); (b) H. Scheingraber and C. R. Vidal, J. Opt. Soc. Am. B **2**, 343 (1985).
[53] R. E. Smalley, L. Wharton, and D. H. Levy, J. Chem. Phys. **63**, 4977 (1975).
[54] (a) F. H. Mies and M. Krauss, J. Chem. Phys. **45**, 4455 (1966); (b) F. H. Mies, Phys. Rev. **175**, 164 (1968).
[55] H. Reisler and C. Wittig, in *Advances in Chemical Kinetics and Dynamics*, edited by R. Barker (JAI, Greenwich, CT, 1992), Vol. 1.
[56] S. Klippenstein, L. R. Khundkar, A. H. Zewail, and R. A. Marcus, J. Chem. Phys. **89**, 4761 (1988).
[57] T. Ericson, Phys. Rev. Lett. **5**, 430 (1960).
[58] P. E. Hodgson, *Nuclear Reactions and Nuclear Structure* (Clarendon, Oxford, 1971).
[59] R. W. Shaw, J. C. Norman, R. Vandenbosch, and C. J. Bishop, Phys. Rev. **184**, 1040 (1969).
[60] S. A. Reid, M. A. Hunter, D. C. Robie, and H. Reisler (to be published).
[61] R. L. Miller, S. H. Kable, P. L. Houston, and I. Burak, J. Chem. Phys. **96**, 32 (1992).
[62] T. Suzuki, V. P. Hradil, S. A. Hewitt, P. L. Houston, and B. J. Whitaker, Chem. Phys. Lett. **187**, 257 (1991).
[63] I.-C. Chen and C. B. Moore, J. Phys. Chem. **94**, 263 (1990); **94**, 269 (1990).
[64] M. Noble, C. X. W. Qian, H. Reisler, and C. Wittig, J. Chem. Phys. **85**, 5763 (1986).
[65] Y. M. Wu and A. Kupperman, Chem. Phys. Lett. **201**, 178 (1993).